Laser-generated toroidal helium plasmas

Kooij, V.L.

4
Microwave analysis of transient toroidal helium plasmas

We experimentally studied laser-generated, atmospheric pressure, transient toroidal helium plasmas using 57 GHz microwave radiation. By combining interferometric measurements with detailed full-wave finite-element calculations, we estimate, with sub-microsecond temporal resolution, the electron number density and the electron collision rate, for the entire evolution of a toroidal plasma. We discuss in detail the microwave interferometric set-up used to measure the complex transmission coefficient, and explain a method whereby the finite-element calculations are used as a map between the measured transmission coefficient and the desired plasma parameters. We briefly discuss an improvement of this method by which a tomographically reconstructed, poloidal intensity profile, based on optical recordings, can be used to better model the toroidal plasma in the finite-element calculations.

4.1 Introduction

In the previous chapters we have examined self-organising toroidal plasmas, generated by a laser-induced breakdown plasma in quiescent atmospheric pressure helium gas at room temperature. We proposed that these transient toroidal helium plasmas might be a first step towards the experimental realisation of self-organising knotted magnetic structures in plasma.[1] Furthermore, the apparent universality of these structures suggests that they may provide the sought after stability in magnetic confinement fusion experiments, and that they might emerge naturally in astrophysical environments.[2]

[1] See section 2.1.

[2] Smiet 2017; Smiet, de Blank et al. 2019.

The prime plasma parameters of interest in any plasma experiment are the electron number density and the electron collision rate. In this chapter, aimed at obtaining these parameters for the entire evolution of our transient toroidal helium plasma, we present interferometric measurements using 57 GHz microwave radiation, and detailed full-

wave finite-element calculations of our interferometric set-up.

The microwave interferometric measurements encode information on the complex permittivity of our toroidal plasma, from which we can derive an estimate of the electron number density and the electron collision rate using the Drude-Lorentz model for electrical conductivity.

Alternative techniques that complement the microwave techniques presented here are Rayleigh and Thomson scattering.[3] Motivated by the expertise present in our group we opted to use microwave technology. Although the spatial resolution is not expected to be comparable to that of Rayleigh and Thomson scattering, which additionally provides information on the electron temperature in a more direct fashion, our choice was equally motivated by our long-term objective to sustain the toroidal plasma through heating using microwave technology. We do expect that our method will depend very critically on the geometry of the plasma when cut-off electron densities are encountered.

[3] Pokrzywka et al. 2012; Nedanovska et al. 2015.

The biggest challenges in our study of transient toroidal helium plasmas are their limited lifetime, which is considerably less than 100 µs, and their limited size, which is of the same order of magnitude as the wavelength of the utilised microwave radiation. The latter implies that the complex transmission coefficient measured by the microwave interferometer depends in a non-trivial way on the complex permittivity of the toroidal plasma.

Our[4] approach to solving these two difficulties is to combine the interferometric measurements with detailed full-wave finite-element calculations. We will discuss the microwave interferometric set-up used to measure the complex transmission coefficient in detail first, and then explain a method whereby the finite-element calculations are used as a map between the measured transmission coefficient and the sought after plasma parameters.

[4] The described method for determining the electron number density and electron collision rate was developed by F.M.A. Smits and has been implemented and utilised in close collaboration with the author of this dissertation.

In our calculations of the complex transmission coefficient we have approximated the toroidal plasma by a torus of fixed size and uniform complex permittivity. In further simplifying our calculations, we used tori of two sizes that are representative for the evolution of our toroidal plasma. For each of these different sized tori, full-wave finite-element calculations have been performed for a range of values for the complex permittivity, or equivalently, for a range of electron number densities and electron collision rates.

These simplifications obviously are a course approximation, but it does provide us with a tractable means to obtain an estimate for the plasma parameters with high temporal resolution. To improve upon this we suggest a method by which a tomographically reconstructed,

poloidal intensity profile, based on optical recordings, can be used to better model the toroidal plasma in the finite-element calculations.

The toroidal plasmas studied in this work have been generated by a single laser-induced breakdown plasma, in quiescent atmospheric pressure helium gas at room temperature, using a laser pulse energy of 250 mJ.

4.2 *Electromagnetic waves in plasma*

Prior to concentrating on the measurement techniques employed to determine the plasma parameters of the toroidal plasma, it is instructive to introduce some fundamental concepts from plasma physics, and discuss in a more general manner the propagation of electromagnetic waves in plasma.

Plasma oscillations

One of the intricate properties of plasma is the rapid oscillation of its electrons.[5] The origin of these plasma oscillations can be understood[6] by considering electrons that are displaced with respect to the uniform ion charge density. It is assumed that, because of their larger mass, the ions form a uniform and stationary charge density. As a consequence of the electron displacement, the resulting electric field will accelerate the electrons back to their original position. However, due to their acquired momentum, the electrons will overshoot and start to oscillate around their equilibrium position, with a characteristic frequency known as the plasma frequency. We can express this mathematically as follows.

[5] Tonks et al. 1929.

[6] Here we loosely follow F. F. Chen 1974, p. 70; Wesson 2004, p. 38.

The balance of momentum[7] for the electron fluid in a cold plasma[8] is given by

$$m_e n_e \frac{D\boldsymbol{u_e}}{Dt} = -e n_e \boldsymbol{E} \tag{4.1}$$

[7] Chorin et al. 1993, p. 6.

[8] For a cold plasma the $-\boldsymbol{\nabla} p$ pressure term in the balance of momentum is negligible.

where m_e is the electron mass, n_e the electron number density, $\boldsymbol{u_e}$ the electron fluid velocity, e the elementary charge, $\boldsymbol{E}$ the electric field, and $D/Dt = \partial/\partial t + \boldsymbol{u_e} \cdot \boldsymbol{\nabla}$ the material derivative. In this equation we recognise Newton's second law of motion and the Lorentz force in absence of a magnetic field.

We assume that the electron density n_e can be separated into an equilibrium density n_0 and a small density perturbation n_1. Then the electric field is given by

$$\boldsymbol{\nabla} \cdot \boldsymbol{E} = -\frac{e}{\epsilon_0} n_1. \tag{4.2}$$

After taking the divergence of equation 4.1 and eliminating $\nabla \cdot \boldsymbol{E}$ through equation 4.2 we have

$$m_e \frac{\partial}{\partial t} \nabla \cdot \boldsymbol{u_e} = \frac{e^2}{\epsilon_0} n_1 \tag{4.3}$$

where the quadratic term $(\boldsymbol{u_e} \cdot \nabla)\boldsymbol{u_e}$ originating from the material derivative has been neglected as a consequence of our perturbative approach.

[9] Chorin et al. 1993, p. 11.

The conservation of mass[9] for the electron fluid is given by

$$\frac{D}{Dt} m_e n_e + m_e n_e \nabla \cdot \boldsymbol{u_e} = 0. \tag{4.4}$$

When we realise that $\partial n_0 / \partial t = 0$ and $\nabla n_0 = 0$, and neglect quadratic terms, then we may write

$$\frac{\partial n_1}{\partial t} + n_0 \nabla \cdot \boldsymbol{u_e} = 0. \tag{4.5}$$

Substitution of $\nabla \cdot \boldsymbol{u_e}$ from equation 4.5 into equation 4.3 results in the differential equation of a simple harmonic oscillator for the electron density perturbation n_1

$$\frac{\partial^2 n_1}{\partial t^2} = -\omega_p^2 n_1$$

where ω_p is the plasma frequency given by

$$\omega_p \equiv \sqrt{\frac{n_0 e^2}{\epsilon_0 m_e}}. \tag{4.6}$$

Note that we cannot explain the plasma oscillations from single particle motion alone, it is necessary to consider the electrons as a fluid. This can be understood when we realise that although the electric field is created as a result of a small perturbation n_1 it is the whole electron fluid with density n_0 that will be set in motion. The plasma frequency therefore only depends on the equilibrium electron number density n_0. It is one of the most fundamental parameters of plasma physics.

Drude-Lorentz model for electrical conductivity

In deriving the plasma frequency we have neglected collisions between electrons and ions, and between the electrons themselves for that matter. These collisions however are responsible for many intricate plasma transport processes, and electrical conductivity is one of them. Without diving into a detailed discourse explaining electrical conductivity, it is possible to convey the essentials through an elementary model first

proposed by Drude.[10]

[10] Drude 1900.

Let us assume once more that, because of their larger mass, the ions form a uniform and stationary density. The electrons will consequently be solely responsible for the transport of electrical current through the plasma. Electrical conductivity manifests itself most recognisable through Joule heating, where the electrons, through collisions, lose kinetic energy to the ions and neutrals. Assume there is some unknown instantaneous collision mechanism maintaining local thermodynamic equilibrium, and that the probability per unit time for such a collision to take place equals $1/\tau$. Maintaining local thermodynamic equilibrium simply means that immediately after each collision, the electron velocity is solely prescribed by the local temperature and is therefore independent of the velocity just before the collision. Further assume that between collisions the electrons only interact with an externally applied electric field and that other interactions can be neglected.[11]

[11] The electron-ion interaction is not completely neglected, it is still implicitly assumed that the electrons remain confined to the quasi-neutral plasma. See Ashcroft et al. 1976, p. 4.

The assumption of local thermodynamic equilibrium implies that the momentum lost per electron per collision is equal to $m_e \boldsymbol{u_e}$. We also assumed that the probability per unit time an electron experiences a collision is equal to $1/\tau$ implying a relaxation or collision time of τ. Consequently, the rate of change of momentum of the electron fluid is given by $m_e n_e \boldsymbol{u_e}/\tau$. The balance of momentum for the electron fluid for a cold plasma is then given by[12]

[12] F. F. Chen 1974, p. 56.

$$m_e n_e \frac{D\boldsymbol{u_e}}{Dt} = -e n_e \boldsymbol{E} - \frac{m_e n_e \boldsymbol{u_e}}{\tau}.$$

This equation simply states that the effect of the electron collisions is to introduce a frictional damping term, in addition to the electromagnetic driving term introduced in the derivation of the plasma frequency. Using the conservation of mass given by equation 4.4 we have[13]

[13] Chorin et al. 1993, p. 7.

$$\begin{aligned}\frac{\partial}{\partial t}(m_e n_e \boldsymbol{u_e}) = &-\boldsymbol{\nabla} \cdot (m_e n_e \boldsymbol{u_e})\boldsymbol{u_e} \\ &- m_e n_e (\boldsymbol{u_e} \cdot \boldsymbol{\nabla})\boldsymbol{u_e} - e n_e \boldsymbol{E} - \frac{m_e n_e \boldsymbol{u_e}}{\tau}.\end{aligned}$$

Neglecting quadratic terms in $\boldsymbol{u_e}$ and assuming that the electron density n_e equals the equilibrium electron density n_0 results in

$$\frac{\partial}{\partial t}(m_e n_0 \boldsymbol{u_e}) = -e n_0 \boldsymbol{E} - \frac{m_e n_0 \boldsymbol{u_e}}{\tau}.$$

Since the current density $\boldsymbol{j}$ is defined as $\boldsymbol{j} \equiv -e n_0 \boldsymbol{u_e}$ we may write

$$\frac{\partial}{\partial t}\boldsymbol{j} = \epsilon_0 \omega_p^2 \boldsymbol{E} - \frac{\boldsymbol{j}}{\tau}$$

where ω_p is the plasma frequency defined in equation 4.6. When we

assume that solutions have a harmonic time dependence $e^{-i\omega t}$ we can write $\boldsymbol{E}(t) = \boldsymbol{E}\,e^{-i\omega t}$ and $\boldsymbol{j}(t) = \boldsymbol{j}\,e^{-i\omega t}$, and find that[14]

$$\boldsymbol{j} = \sigma(\omega)\boldsymbol{E}$$

which is Ohm's law of electrical conductivity, where $\sigma(\omega)$ is the electrical conductivity given by

$$\sigma(\omega) = \frac{\sigma_0}{1 - i\omega\tau} \qquad \text{where} \qquad \sigma_0 = \epsilon_0\omega_p^2\tau = \frac{n_0e^2\tau}{m_e}. \tag{4.7}$$

At zero frequency, the electrical conductivity $\sigma(\omega)$ reduces to the direct-current Drude conductivity σ_0.

[14] Throughout this chapter we use the quantum mechanical sign convention, where a wave propagating in the $\boldsymbol{k}$ direction for $\omega > 0$ is represented by $e^{i\boldsymbol{k}\cdot\boldsymbol{x}-i\omega t}$.

Electromagnetic waves in linear media

The propagation of electromagnetic waves is an extensive subject about which many works have been written.[15] For the purpose of this section we will only consider the propagation of plane electromagnetic waves in linear media and underline the equivalence of describing linear media by, for example, the dispersion relation, the complex permittivity, or the electrical conductivity.

[15] See for example Jackson 1998; Griffiths 1999, and references therein.

For uniform isotropic linear media the Maxwell equations[16] for a charge-free infinite medium are

$$\nabla\cdot\boldsymbol{E} = 0 \qquad \nabla\times\boldsymbol{E} = -\frac{\partial\boldsymbol{B}}{\partial t}$$
$$\nabla\cdot\boldsymbol{B} = 0 \qquad \nabla\times\boldsymbol{B} = \mu\boldsymbol{j} + \mu\epsilon\frac{\partial\boldsymbol{E}}{\partial t}$$

where the permeability μ and the permittivity ϵ describe our linear medium and may in general be complex functions. When we assume that solutions have a harmonic time dependence $e^{-i\omega t}$ we can write $\boldsymbol{E}(t) = \boldsymbol{E}\,e^{-i\omega t}$, $\boldsymbol{B}(t) = \boldsymbol{B}\,e^{-i\omega t}$ and $\boldsymbol{j}(t) = \boldsymbol{j}\,e^{-i\omega t}$, and the Maxwell equations turn into

$$\nabla\cdot\boldsymbol{E} = 0 \qquad \nabla\times\boldsymbol{E} = i\omega\boldsymbol{B}$$
$$\nabla\cdot\boldsymbol{B} = 0 \qquad \nabla\times\boldsymbol{B} = \mu\boldsymbol{j} - i\mu\epsilon\omega\boldsymbol{E}.$$

When we take the curl of the equation for $\nabla\times\boldsymbol{E}$ and eliminate $\nabla\times\boldsymbol{B}$, then we can write

$$\nabla\times(\nabla\times\boldsymbol{E}) = \mu\epsilon\omega^2\boldsymbol{E} + i\mu\omega\boldsymbol{j}.$$

Using the vector calculus identity $\nabla\times(\nabla\times\boldsymbol{A}) = \nabla(\nabla\cdot\boldsymbol{A}) - \nabla^2\boldsymbol{A}$,

[16] Jackson 1998, pp. 238 and 295. For uniform isotropic linear media the commonly used fields $\boldsymbol{D}$ and $\boldsymbol{H}$ can be written as $\boldsymbol{D} = \epsilon\boldsymbol{E}$ and $\boldsymbol{B} = \mu\boldsymbol{H}$. In that context $\boldsymbol{H}$ is called the magnetic field and $\boldsymbol{B}$ is called the magnetic induction.

realising $\boldsymbol{\nabla} \cdot \boldsymbol{E}$ is equal to zero, and substituting Ohm's law of electrical conductivity[17,18] $\boldsymbol{j} = \sigma(\omega)\boldsymbol{E}$, we arrive at the Helmholtz wave equation

$$\boldsymbol{\nabla}^2 \boldsymbol{E} + \mu\epsilon \left(1 + i\frac{\sigma}{\epsilon\omega}\right) \omega^2 \boldsymbol{E} = 0.$$

A possible solution is a plane electromagnetic wave $e^{i\boldsymbol{k}\cdot\boldsymbol{x} - i\omega t}$ propagating in the $\boldsymbol{k}$ direction for $\omega > 0$. From the Helmholtz wave equation we then find the requirement that the wave number $k = |\boldsymbol{k}|$ and the frequency ω are related by

$$k^2 = \mu\epsilon \left(1 + i\frac{\sigma}{\epsilon\omega}\right) \omega^2.$$

This is the dispersion relation for electromagnetic waves propagating in uniform isotropic linear media.

Generally, a dispersion relation relates the wave number k of a propagating wave to its frequency ω, and is universally written as $\omega(k) = v(k)\, k$, where $v(k)$ is the propagation speed or phase velocity.[19] It is important to realise that the propagation of electromagnetic waves in linear media is completely determined by the dispersion relation and that it represents all properties of our linear medium, regardless of whether they originate from the permeability μ, the permittivity ϵ, or the electrical conductivity σ. It is merely a choice by which measure we wish to represent our linear medium.

As an example, assume our medium lacks both polarisation as well as magnetic[20] properties, implying $\epsilon = \epsilon_0$ and $\mu = \mu_0$, and that we opt to represent its electrical conductivity σ solely by an equivalent complex permittivity $\widetilde{\epsilon}$, hence $\widetilde{\mu} = \mu_0$ and $\widetilde{\sigma} = 0$. Then we can write the dispersion relation of our medium and its equivalent representation respectively as

$$k^2 = \mu_0\epsilon_0 \left(1 + i\frac{\sigma}{\epsilon_0\omega}\right) \omega^2$$

and

$$k^2 = \mu_0\widetilde{\epsilon}\omega^2. \tag{4.8}$$

Evidently we have

$$\widetilde{\epsilon} = \epsilon_0 \left(1 + i\frac{\sigma}{\epsilon_0\omega}\right) \tag{4.9}$$

which provides an equally apt representation of our electrically conductive linear medium in terms of an equivalent complex permittivity.

[17] We assume that a dc magnetic field is absent so Ohm's law may be applied. In the presence of a dc magnetic field this is no longer true as the Hall effect and magneto-resistance become important.

[18] The Drude-Lorentz model has been derived assuming a constant electric field $\boldsymbol{E}$. It is not evident that the electrical conductivity thus found is applicable in our context of a spatially varying electric field. However, if the electric field does not vary appreciably over distances comparable to the electron mean free path, we can write the current density $\boldsymbol{j}$ as $\boldsymbol{j}(\boldsymbol{r},\omega) = \sigma(\omega)\boldsymbol{E}(\boldsymbol{r},\omega)$. See Ashcroft et al. 1976, p. 17.

[19] An associated quantity, the complex refractive index n, relates the propagation speed in free space ($\mu = \mu_0$, $\epsilon = \epsilon_0$, and $\sigma = 0$) to the propagation speed in the linear medium, and can be defined through $n \equiv k/k_0$, where $k_0 \equiv \omega\sqrt{\mu_0\epsilon_0}$ is the wave number in free space. Because k and n are on an equal footing, for the sake of clarity, we deliberately omit the complex refractive index n.

[20] In magnetic media the permeability μ is no longer equal to the permeability μ_0 of free space as a result of the induced magnetisation in response to an external magnetic field.

The wave number k and the equivalent complex permittivity $\widetilde{\epsilon}$ are related through the equivalent dispersion relation 4.8 and universally their real and imaginary parts are explicitly written

$$k \equiv k' + i\,k''$$
$$\widetilde{\epsilon} \equiv \widetilde{\epsilon}' + i\,\widetilde{\epsilon}''.$$

From the equivalent dispersion relation 4.8 we have[21]

$$k = k_0 \sqrt{\frac{\widetilde{\epsilon}}{\epsilon_0}}$$

where $k_0 \equiv \omega\sqrt{\mu_0\epsilon_0}$ is the wave number in free space. The principal square root can be expressed algebraically[22] so we can write[23]

$$k' = k_0 \sqrt{\frac{|\widetilde{\epsilon}| + \widetilde{\epsilon}'}{2\,\epsilon_0}} \tag{4.10}$$

$$k'' = k_0 \sqrt{\frac{|\widetilde{\epsilon}| - \widetilde{\epsilon}'}{2\,\epsilon_0}}. \tag{4.11}$$

When considering the propagation of a plane electromagnetic wave, we can assume, without loss of generality, that the propagation is in the x-direction. Then we can write

$$e^{ikx - i\omega t} = e^{i(k' + i\,k'')x - i\omega t} = e^{-k''x}\, e^{ik'x - i\omega t}.$$

Evidently our electromagnetic wave attenuates exponentially with attenuation constant k'' while propagating with wave number k'.

[21] In terms of the complex refractive index n introduced earlier we have $n = \sqrt{\widetilde{\epsilon}/\epsilon_0}$.

[22] Abramowitz et al. 1972, p. 17.

[23] There exists ambiguity regarding the sign of the imaginary part of the principal square root and the imaginary parts of k and $\widetilde{\epsilon}$. Here $k'' > 0$ and $\widetilde{\epsilon}'' > 0$ represent loss where the electromagnetic wave attenuates exponentially. Similarly $k' > 0$ represents propagation in the $\boldsymbol{k}$ direction for $\omega > 0$.

Plasma complex permittivity and electromagnetic wave propagation

In the previous sections we have gained some[24] insight into the rapid oscillation of electrons in plasma and the Drude-Lorentz model for electrical conductivity, and appreciated the equivalence in representing uniform isotropic linear media. Here, we will apply these insights to the complex permittivity of plasma and the propagation of electromagnetic waves in plasma.

The electrical conductivity $\sigma(\omega)$ obtained through the Drude-Lorentz model is given by equation 4.7 and can be written as

$$\sigma(\omega) = \frac{\epsilon_0 \omega_p^2 \tau}{1 - i\omega\tau}$$

when we substitute the direct-current Drude conductivity σ_0. Then the

[24] Trivially, we have examined only some of the countless intricate properties of plasma. See F. F. Chen 1974; Bellan 2006; Goedbloed et al. 2004; Kulsrud 2005 for more detailed works. For a condensed matter physics perspective the reader might consult Marder 2010.

equivalent complex permittivity $\widetilde{\epsilon}$ given by equation 4.9 can be written as

$$\frac{\widetilde{\epsilon}}{\epsilon_0} = 1 - \frac{n_0}{n_c} \frac{1}{1 + i\frac{\nu}{\omega}}$$

where we introduced the electron collision rate $\nu \equiv 1/\tau$ and the critical electron number density[25] $n_c \equiv \epsilon_0 m_e \omega^2 / e^2$. The real part of the equivalent complex permittivity $\widetilde{\epsilon}$ can be written as

$$\frac{\widetilde{\epsilon}'}{\epsilon_0} = 1 - \frac{n_0}{n_c} \frac{1}{1 + \left(\frac{\nu}{\omega}\right)^2}$$

while its imaginary part takes the form

$$\frac{\widetilde{\epsilon}''}{\epsilon_0} = \frac{n_0}{n_c} \frac{\frac{\nu}{\omega}}{1 + \left(\frac{\nu}{\omega}\right)^2}.$$

The imaginary part makes it evident that a non-zero electron collision rate ν results, as expected, in loss represented by $\widetilde{\epsilon}'' > 0$. The behaviour of an electromagnetic wave propagating through the plasma is easily obtained through equations 4.10 and 4.11 relating the real and imaginary parts of k and $\widetilde{\epsilon}$.

We conclude this section by presenting in figure 4.1 the normalised[26] real and imaginary part k'/k_0 and k''/k_0 of wave number k, as a function of the normalised electron number density n_0/n_c and the normalised electron collision rate ν/ω. From these, two observations are noteworthy.

When electron collisions are negligible ($\nu = 0$) then, for electron number densities larger than the critical density ($n_0 > n_c$), the real part k' becomes zero, while the imaginary part k'' acquires a finite value. The equivalent complex permittivity turns negative, hence the wave number becomes purely imaginary and propagation is not possible. We speak of an evanescent wave. For electron number densities smaller than the critical density ($n_0 < n_c$) wave propagating is lossless with a phase velocity exceeding the speed of light in vacuum.

When electron collisions are present ($\nu \neq 0$) propagation is possible for all electron number densities. Intuitively this can be understood by realising that, due to their collisions, the electrons are limited in their movement and are no longer able to fully respond to the applied electromagnetic field.

[25] At a constant frequency ω the equivalent complex permittivity $\widetilde{\epsilon}$ becomes zero when the electron number density n_0 is equal to the critical electron number density given by $n_c \equiv \epsilon_0 m_e \omega^2 / e^2$. Precisely at the critical electron number density we have $\omega_p = \omega$. See F. F. Chen 1974, p. 103.

[26] In figure 4.1 we normalised to k_0 and essentially present the real and imaginary part of the complex refractive index introduced earlier.

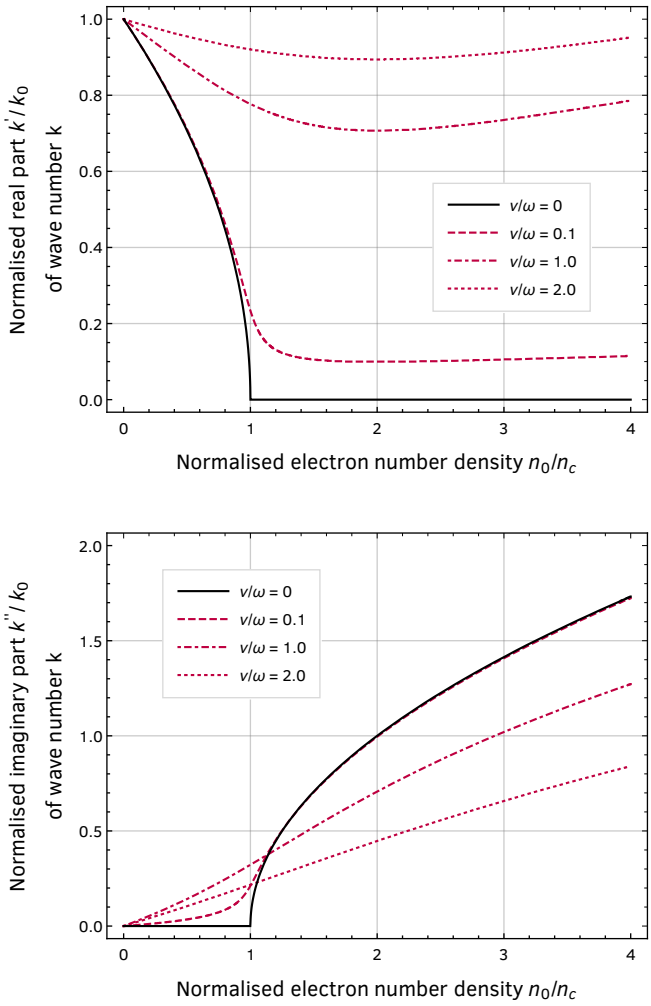

Figure 4.1: Normalised real part k'/k_0 and imaginary part k''/k_0 of wave number k, as a function of the normalised electron number density n_0/n_c and the normalised electron collision rate ν/ω.

4.3 *Microwave analysis of transient toroidal helium plasmas*

The prime plasma parameters of interest in any plasma experiment are the electron number density and the electron collision rate of the plasma under consideration. In this section we present microwave interferometric measurements at 57 GHz, aimed at obtaining these parameters, with high temporal resolution, for the whole evolution of our transient toroidal helium plasma. These measurements encode

information on the complex transmission coefficient for microwaves traversing our toroidal plasma, which in itself contains information about the complex permittivity of the plasma. From this, we can derive an estimate of the electron number density and the electron collision rate through the Drude-Lorentz model for electrical conductivity.

The propagation of electromagnetic waves through a voluminous plasma is straightforward, and for these plasmas the expressions presented in section 4.2 can be utilised safely to obtain the electron number density and the electron collision rate from the measured complex permittivity of the plasma. Unfortunately, this simple strategy is not applicable to our toroidal plasma. The wavelength of the utilised microwave radiation is 5.3 mm, which is of the same order of magnitude as the size of our toroidal plasma, as can be seen from our measurements presented in section 2.3. The complex transmission coefficient measured by the microwave interferometer therefore depends on the complex permittivity in a non-trivial way.[27]

[27] The small separation of the horn antennas used for the transmission measurements further complicates the determination of the complex transmission coefficient, because of multiple reflections of the microwave radiation between these antennas.

Our approach to solving this difficulty is to perform complex transmission measurements using a microwave interferometer, and to subsequently compare these measurements to electromagnetic full-wave finite-element calculations of the interferometric set-up, including a torus mimicking our toroidal plasma. The complex transmission coefficient calculated in this manner for a set of tori, each with a different complex permittivity, can be used as a map to obtain the complex permittivity of our toroidal plasma as a function of time.

Because the finite-element calculations already are computationally intensive, we have approximated our toroidal plasma by a torus of fixed dimensions and uniform complex permittivity. This necessarily is a coarse approximation, but it does provide, with high temporal resolution, a first estimate of the electron number density and the electron collision rate as a function of time.

Examination of the microwave interferometer

A simplified schematic[28] of the microwave interferometric set-up is presented in figure 4.2. Microwave radiation, generated using a 57 GHz 100 mW Gunn oscillator, is guided through rectangular TE10 mode wave-guide with dimensions of 3.76 x 1.88 mm, to a 10 dB directional coupler, were it is split into a reference and transmission signal. The reference signal is guided through an adjustable attenuator while the transmission signal is fed into a copper pyramidal horn antenna with an apex-aperture distance of 45 mm and an aperture of 18 x 11 mm.

[28] For a more lively impression of the experimental set-up we refer to photo 2 on page 104.

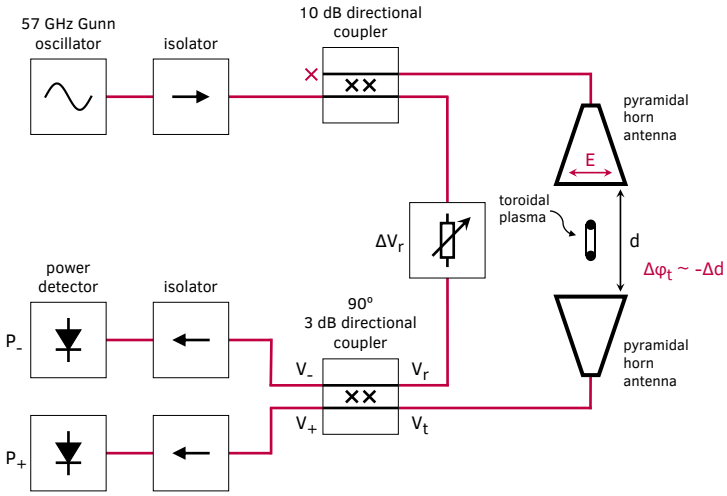

Figure 4.2: Simplified schematic of the microwave interferometric set-up used to measure the complex transmission coefficient of our transient toroidal helium plasma with high temporal resolution. See text for details. For a more lively impression of the experimental set-up we refer to photo 2 on page 104.

This horn antenna couples the microwave radiation into free space, which subsequently traverses the toroidal plasma before it is received by a second identical pyramidal horn antenna. The horn antennas are separated by a distance of 24.3 mm.

The reference and transmission signals are recombined using a 90° 3 dB directional coupler[29] whose output ports are equipped with a microwave power detector. The attenuator can be used to reduce the power of the reference signal, while the phase between the reference and transmission signals can be adjusted by changing the distance between the horn antennas. Microwave isolators have been used to prevent interference arising from reflections from the power detectors, the pyramidal horn antennas, and the toroidal plasma. The power detectors have been calibrated to correct for their non-linear power to voltage response.

[29] A directional coupler designed for a 3 dB power split is known as a hybrid coupler.

We note that the whole microwave interferometric set-up has been mounted inside our plasma reactor. Because of the large number of components, degassing becomes an issue and long evacuation times are needed to remove the air from our plasma reactor. This is not the most ideal approach, but it proved to be the most practical means to integrate these measurements into our existing set-up for the generation of toroidal helium plasmas.

The central component of the interferometric set-up is the 90° 3 dB directional coupler. When all ports of a 90° 3 dB directional coupler are

connected to matched wave-guides, and microwaves are assumed not to traverse the coupler in the reverse direction, implying ideal microwave isolators, then the voltages of the ports of the coupler are given by[30,31,†]

$$\begin{bmatrix} V_+ \\ V_- \end{bmatrix} = \frac{1}{\sqrt{2}} \begin{bmatrix} 1 & i \\ i & 1 \end{bmatrix} \begin{bmatrix} V_t \\ V_r \end{bmatrix}$$

where V_+ and V_- are the power detector input voltages, V_t is the transmitted voltage after the microwave radiation has traversed the toroidal plasma, and V_r is the reference voltage. When we assume that the impedances are normalised to 1 Ohm, then for all voltages in our set-up, the time-averaged power is given by $P = \frac{1}{2}|V|^2$. The power received by the microwave detectors is then given by

$$P_+ = \frac{1}{4}\,|V_t + iV_r|^2$$
$$P_- = \frac{1}{4}\,|V_t - iV_r|^2\,.$$

The reference voltage V_r can be obtained in the following manner, while calibrating the interferometric set-up. Let us use a superscript label (cal) to denote an empty interferometer during this calibration. We can adjust the attenuation of the reference signal, and the phase between the reference and transmitted signals, in such a way that detector signal P_- becomes zero, implying we have ${V_t}^{cal} = i{V_r}^{cal}$. Consequently we have

$$P_t^{cal} = P_r^{cal} \tag{4.12}$$

and

$$P_+^{cal} = 2P_r^{cal}$$
$$P_-^{cal} = 0\,.$$

[30] Collin 2001, p. 413.

[31] The matrix in this equation is a reduced scattering matrix, where the matrix elements representing microwaves traversing the directional coupler in the reverse direction have been omitted.

[†] In general the scattering matrix of a 3 dB directional coupler can be written as

$$[S] = \frac{1}{\sqrt{2}} \begin{bmatrix} 0 & 0 & 1 & e^{i\alpha} \\ 0 & 0 & -e^{-i\alpha} & 1 \\ 1 & -e^{-i\alpha} & 0 & 0 \\ e^{i\alpha} & 1 & 0 & 0 \end{bmatrix}$$

where $\alpha \in \mathbb{R}$ defines the phase difference between the output ports. Unfortunately the sign of α is not always known. Moreover, the sign convention used to represent a propagating wave affects the scattering matrix, specifically, a scattering matrix defined in one sign convention is the complex conjugate of the other (see Ye et al. 2018). More about sign conventions can be found in Muller 1969; Atkinson et al. 1992. Here we assume $\alpha = \frac{\pi}{2}$. The sign of α is not important, because in an interferometric set-up, where only the change in phase is relevant, all information can be distilled from the behaviour of the power difference $P_+ - P_-$ as a function of the distance d between the pyramidal horn antennas.

[32] In an interferometric set-up only the phase between the reference and transmitted signals is a meaningful quantity.

Without loss of generality[32] we may assume V_r^{cal} to be positive real valued, so we can write $V_r^{cal} = \sqrt{2P_r^{cal}} = \sqrt{P_+^{cal}}$.

An ideal directional coupler is a lossless component, therefore conservation of energy implies that $P_+ + P_- = P_t + P_r$. For a calibrated interferometer, the power of the microwave radiation traversing the toroidal plasma, and received by the pyramidal horn antenna, is thus

$$P_t = P_+ + P_- - P_r^{cal}. \tag{4.13}$$

Our toroidal plasma will not only attenuate the microwave radiation, it will also change its phase. This change in phase is encoded in the power difference $P_+ - P_-$ measured by the microwave detectors. Using the complex conjugate properties of complex numbers and realising we assumed V_r^{cal} to be positive real valued, we can derive

$$\mathrm{Im}(V_t) = \frac{P_+ - P_-}{V_r^{cal}} \tag{4.14}$$

where $\mathrm{Im}(V_t)$ denotes the imaginary part of V_t. Because $|V_t| = \sqrt{2P_t}$ the phase of V_t can be readily obtained.

Using the interferometer when P_- is adjusted to zero makes the complex transmission measurement insensitive to the sign of the change in phase. This is evident from the fact that when the phase of V_t changes, the transmitted power, and hence the sum $P_+ + P_-$, does not change. As a consequence, the power difference $P_+ - P_-$ will decrease irrespective of the sign of the change in phase.

Ideally this is resolved by setting up the interferometer in such a way that the power difference $P_+ - P_-$ is zero, which can be accomplished by adjusting the phase between the reference and transmitted signals through adjustment of the distance between the pyramidal horn antennas. In this case we immediately see from equation 4.14 that the sign of the power difference $P_+ - P_-$ will be equal to the sign of the change in phase of the transmitted signal. Experimentally this adjustment does not have to be accurate because, as we will show later, we can correct for a non-zero power difference $P_+ - P_-$ as long as $P_- \neq 0$.

Let us use a superscript zero (o) to denote an empty and calibrated microwave interferometer where the power difference $P_+ - P_-$ has been adjusted to zero. The detector signals so defined can be obtained straightforwardly from the recordings of the detector signals, just before a laser-induced breakdown plasma is generated. Realising that the transmitted power does not change while adjusting its phase, we have

$P_t^0 = P_t^{cal}$. Then, by making use of equations 4.12 and 4.13, we can write

$$P_t^0 = \frac{P_+^0 + P_-^0}{2}. \tag{4.15}$$

If we now normalise all power measurements to $P_t^0 = \frac{1}{2}|V_t^0|^2$ and denote these using a tilde (~) and furthermore define the normalised transmitted voltage as $\widetilde{V}_t \equiv V_t/|V_t^0|$ we can write[33]

$$|\widetilde{V}_t| = \sqrt{\widetilde{P}_+ + \widetilde{P}_- - 1}$$
$$\mathrm{Im}(\widetilde{V}_t) = \frac{\widetilde{P}_+ - \widetilde{P}_-}{2}.$$

[33] Note that due to the chosen normalisation $\widetilde{V}_t^0$ is complex for $P_+^0 - P_-^0 \neq 0$. Furthermore $|\widetilde{V}_t^0| = 1$ and $\widetilde{P}_t = |\widetilde{V}_t|^2$.

The normalised transmitted voltage $\widetilde{V}_t$ is easily obtained from these relations and encodes information about the propagation of microwave radiation through our toroidal plasma.[34] When corrected for the phase of $\widetilde{V}_t^0$ it is customary to denote this quantity in microwave technology as the complex transmission coefficient S_{21}.

[34] Due to the small separation of the pyramidal horn antennas, multiple reflections between these antennas inevitably affects the complex transmission coefficient determined in this experiment.

The normalised transmitted voltage $\widetilde{V}_t$ is not uniquely defined through $|\widetilde{V}_t|$ and $\mathrm{Im}(\widetilde{V}_t)$ because the sign of the real part of $\widetilde{V}_t$ is not known. In figure 4.3 we illustrate this ambiguity by showing the simulated normalised detector signals $\widetilde{P}_+$ and $\widetilde{P}_-$ of a 90° 3 dB directional coupler as a function of the phase between V_t and V_r. The non-zero power difference $\widetilde{P}_+^0 - \widetilde{P}_-^0$ for the empty and calibrated microwave interferometer has been chosen arbitrarily. It is clear that

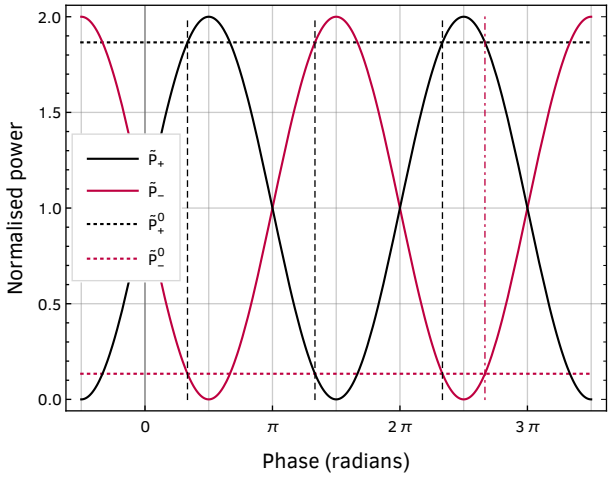

Figure 4.3: Illustration of the ambiguity in the determination of the phase of $\widetilde{V}_t$ due to the unknown sign of the real part of $\widetilde{V}_t$. See text for a detailed discussion.

the horizontal dashed black line $\widetilde{P}_+^0$ intersects the black sine $\widetilde{P}_+$ at two phase angles, reflecting the two possibilities for the real part of $\widetilde{V}_t$. An experimental analysis of the behaviour of the power difference $\widetilde{P}_+ - \widetilde{P}_-$ as a function of the distance d between the pyramidal horn antennas will determine whether the real part is positive or negative. When the horn antenna distance is decreased, the phase between V_t and V_r increases. If at the same time $\widetilde{P}_+ - \widetilde{P}_-$ increases, the real part of $\widetilde{V}_t$ is positive.[35]

[35] Note that exchanging the detector signals P_+ and P_- is equivalent to adding π to the phase between V_t and V_r. Furthermore, recall that the exact scattering matrix of the directional coupler, as well as the exact length of the guides, are not known. As a result, only changes in the phase between V_t and V_r due to our toroidal plasma, are a meaningful quantity. Without loss of generality we can therefore assume that $P_+ > P_-$.

Microwave interferometric complex transmission measurements

Using the experimental set-up and method set out in the previous subsection, we performed complex transmission measurements on our transient toroidal helium plasma, generated by a single laser-induced breakdown plasma. These breakdown plasmas have been created in quiescent atmospheric pressure helium gas at room temperature, with a laser pulse energy of 250 mJ, using a 1" plano-convex lens with a focal length of 50 mm. In section 2.3 it has been shown that the evolution of these plasmas is very reproducible. In order to increase the signal to noise ratio, most notably during the faint afterglow, therefore all

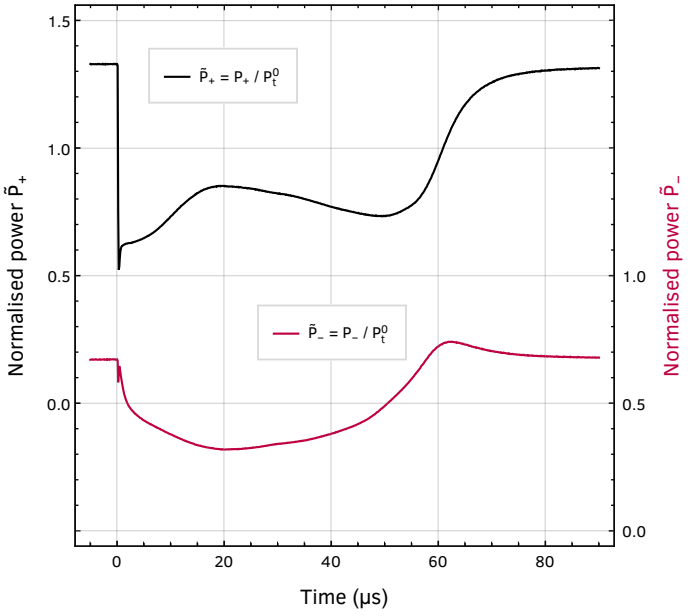

Figure 4.4: Normalised microwave detector signals $\widetilde{P}_+$ and $\widetilde{P}_-$ recorded during a complex transmission measurement on a transient toroidal helium plasma, generated by a laser-induced breakdown plasma created in quiescent atmospheric pressure helium gas at room temperature. Laser pulse energy: 250 mJ, focal length focussing lens: 50 mm, helium gas pressure: 1000 mbar, microwave detector signal averaging: 100.

recordings of the microwave detector signals have been averaged over 100 repetitions.

In figure 4.4 we present the recorded microwave detector signals normalised to P_t^0 as defined in equation 4.15. The values for P_+^0 and P_-^0 have been obtained from the same recordings at 0 µs, just before a laser-induced breakdown plasma is created.

From these recordings, the magnitude and phase of the complex transmission coefficient S_{21} have been obtained using the method set out in the previous subsection, and are presented in figure 4.5. The fast response visible at 0 µs indicates that measurements can be obtained with high temporal resolution.

Near the end of the evolution, the complex transmission coefficient is seen to return to unity, with a slightly positive but monotonically decreasing phase. This is expected from an extinguishing plasma because, as was shown in section 4.2, plasma with a small electron number density exhibits a wave number k slightly smaller than k_0, the wave number in free space.

Together with full-wave finite-element calculations, these complex transmission measurements will be used to provide, with high temporal

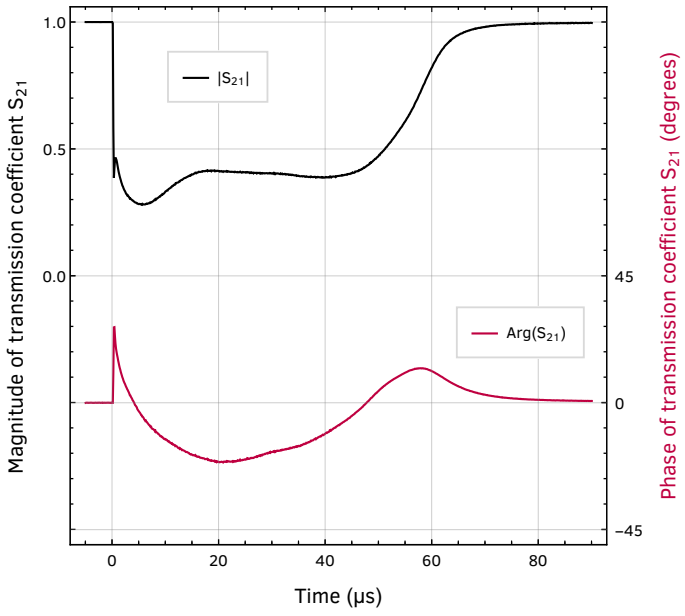

Figure 4.5: High temporal resolution complex transmission coefficient S_{21} obtained through microwave interferometric measurements on a transient toroidal helium plasma, generated by a laser-induced breakdown plasma created in quiescent atmospheric pressure helium gas at room temperature. The complex transmission coefficient has been derived from the recorded microwave detector signals presented in figure 4.4.

resolution, a first estimate of the electron number density and the electron collision rate as a function of time.

Full-wave finite-element complex transmission calculations

For a voluminous plasma the relation between the complex transmission coefficient S_{21} and the complex wave number k, and similar, to the complex permittivity ϵ, and hence to the electron number density and the electron collision rate, is straightforward, and our treatise on the propagation of electromagnetic waves in plasma presented in section 4.2 implies

$$S_{21} = e^{-k'' d}\, e^{i(k_0 - k')\, d}$$

where k' and k'' are respectively the real and imaginary part of the complex wave number, d is the distance the microwave radiation propagates through the voluminous plasma, and k_0 is the wave number of the microwave radiation in free space.

However, as explained in the introduction, the dimensions of our toroidal plasma are of the same order of magnitude as the wavelength of the microwave radiation used to probe the plasma. Therefore, the limit for a voluminous plasma does not hold. Furthermore, because the separation of the pyramidal horn antennas is likewise small compared to the aperture of these antennas, multiple reflections between the horn antennas become important. Our only viable resort to obtain the plasma parameters from the presented complex transmission measurements are full-wave finite-element calculations of our microwave interferometric set-up, including a torus of uniform complex permittivity that is used to mimic our toroidal plasma.

In figure 4.6 we present the geometry used for the finite-element calculations, which shows the pyramidal horn antennas and the torus mimicking our toroidal plasma. A fully absorbing cylindrical surface around the horn antennas and the torus defines the region of free space.

Because the finite-element calculations already are computationally intensive, we have limited the calculation of the complex transmission coefficient to tori of two sizes that are representative for the evolution of our toroidal plasma. These sizes have been obtained from the optical measurements of our toroidal plasma presented in figure 2.8, at 30 µs and 50 µs. These moments respectively lie midway of the expanding phase, and towards the end of the evolution of the toroidal plasma. For each of these different sized tori, full-wave finite-element calculations have been performed for a range of values for the complex permittivity,

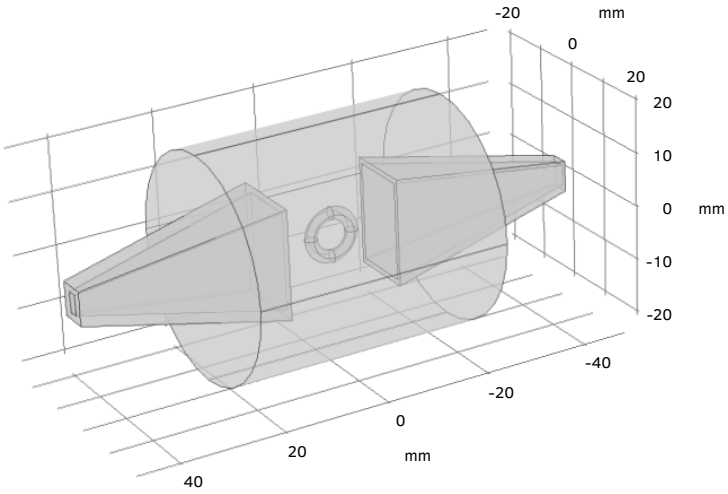

Figure 4.6: Geometry used for the full-wave finite-element calculations showing the pyramidal horn antennas and the torus mimicking our toroidal plasma. A fully absorbing cylindrical surface around the horn antennas and the torus defines the region of free space.

or equivalently, for a range of electron number densities and electron collision rates. These values have been guided by known estimates for atmospheric pressure plasmas generated in the laboratory.[36]

[36] Kabouzi et al. 2002; F. F. Chen 1974; Richardson 2019.

The optical size of the toroidal plasma is expected to be similar to the electrical size determined by the free electrons in the toroidal plasma. However, as electrons are assumed to be responsible for the plasma emission, through collisional excitation of neutral atomic helium, low energy electrons, with insufficient energy to cause excitation of the helium atoms, can have a wider extent than optically observed.

Figure 4.7 presents the electric field strength of two representative finite-element calculations for a normalised electron collision rate ν/ω of 0.8 and a normalised electron number density n_0/n_c of 0.1 and 1.0. Here ν is the electron collision rate, ω is the frequency of the microwave radiation used to probe the toroidal plasma, n_0 is the electron number density, and n_c is the critical electron number density as defined in section 4.2. This figure clearly illustrates the complexity originating from the fact that the wavelength of the microwave radiation used is of the same order of magnitude as the dimensions of the toroidal plasma. It is evident that the behaviour of an electromagnetic wave propagating through such a plasma does not begin to compare with the propagation through a voluminous plasma.

In the presented full-wave finite-element calculations the complex permittivity has been assumed uniform throughout the torus. Ideally,

the poloidal radiant intensity profile, obtained through the three-dimensional tomographic reconstruction presented in section 2.5, is used as a measure for the dimensions and the electron number density of the toroidal plasma. However, the finite-element calculations already are computationally intensive, and with the course approximations applied we still are able to provide a first estimate for the plasma parameters of our toroidal plasma.

The full-wave finite-element calculations performed in the above manner relate the complex transmission coefficient S_{21} to pairs of the electron number density n_0 and the electron collision rate ν. For

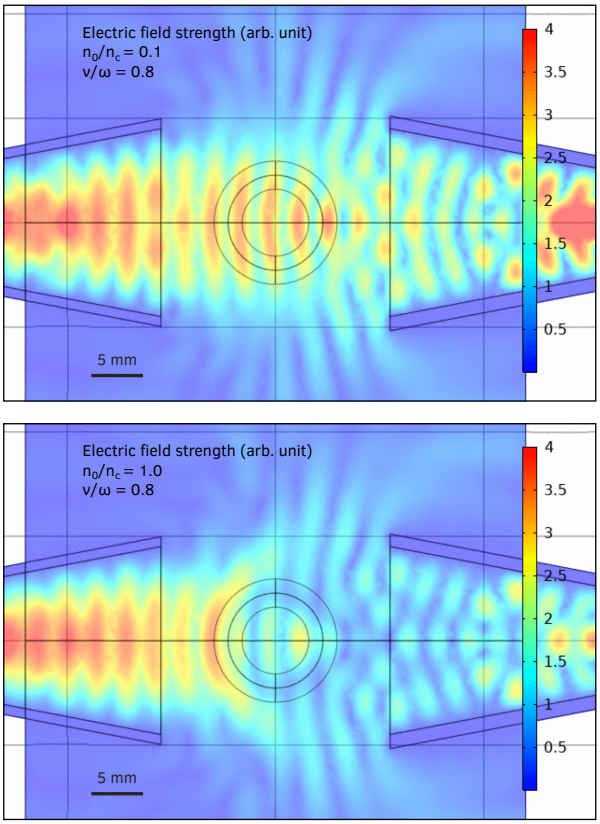

Figure 4.7: Electric field strength of two representative finite-element calculations for a normalised electron collision rate ν/ω of 0.8 and a normalised electron number density n_0/n_c of 0.1 and 1.0, showing the complexity originating from the fact that the wavelength of the microwave radiation used is of the same order of magnitude as the dimensions of the toroidal plasma. Here ν is the electron collision rate, ω is the frequency of the microwave radiation used to probe the toroidal plasma, n_0 is the electron number density, and n_c is the critical electron number density as defined in section 4.2. The torus used to mimic the toroidal plasma in these calculations is represented by the two concentric circles in the centre. The electric field strength is shown for the cross-sectional symmetry plane parallel to the long side of the aperture of the pyramidal horn antennas shown in figure 4.6. As a consequence of the employed TE10 mode, the electric field is directed orthogonal to this symmetry plane.

reasons of readability, the presentation of this relation is postponed to the next subsection, where it will be presented together with high temporal resolution, complex transmission measurements, obtained through the microwave interferometric measurements on our transient toroidal helium plasma.

Electron number density and electron collision rate determination

In the previous sections we have presented high temporal resolution, complex transmission measurements on our transient toroidal helium plasma. We also presented full-wave finite-element calculations of the complex transmission coefficient of our entire experimental set-up, where our toroidal plasma has been mimicked by a uniform torus. In figure 4.8 we present, in the complex plane, the complex transmission coefficient obtained through both these methods. The continuous black curve represents the evolution of the complex transmission coefficient of our toroidal plasma for its entire evolution, while the coloured lines represent the finite-element calculations for different sized tori, and for different electron number densities and electron collision rates.

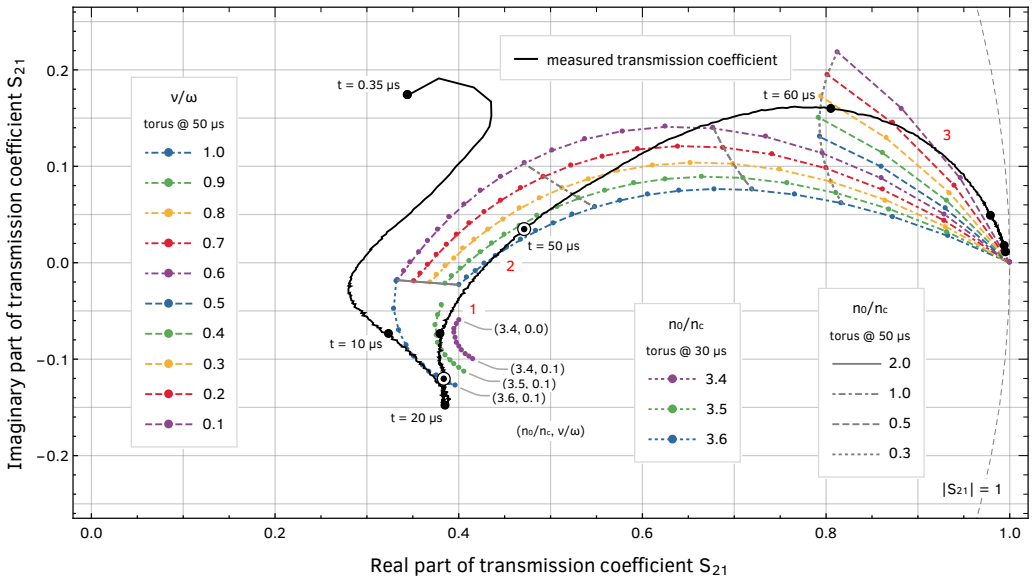

Figure 4.8: Complex transmission coefficient S_{21} obtained for our transient toroidal helium plasma through high temporal resolution complex transmission measurements using a microwave interferometer (continuous black curve with time markers) together with full-wave finite-element calculations of our entire experimental set-up in which our toroidal plasma has been mimicked by a torus of fixed size, and with uniform electron number density and electron collision rate (coloured lines). The bullseye time markers along the black curve, at 30 µs and 50 µs, indicate when the two representative sizes for the evolution of the toroidal plasma have been obtained.

A first estimate of the electron number density and the electron collision rate can now be obtained in high temporal resolution, by regarding the finite-element calculations as a map from the complex plane to the two-dimensional space spanned by the electron number density and the electron collision rate, and subsequently applying this map to the complex transmission coefficient obtained by our microwave interferometric measurements. Because the map resulting from the finite-element calculations is discrete, a linear interpolation has been used to create a continuous map.

In figure 4.9 we present the normalised electron number density and the normalised electron collision rate of our transient toroidal helium plasma, as modelled by a uniform torus and obtained in the manner set out above. It is clear that in the first half of the evolution, the electron number density is well above cut-off. Towards the end of the evolution, the electron number density monotonically decreases to zero, which is, as explained earlier, expected for an extinguishing plasma. In this part of the evolution, the electron number density and the electron collision rate are of the order of 10^{19} m^{-3} respectively 10^{10} s^{-1}, which conforms to

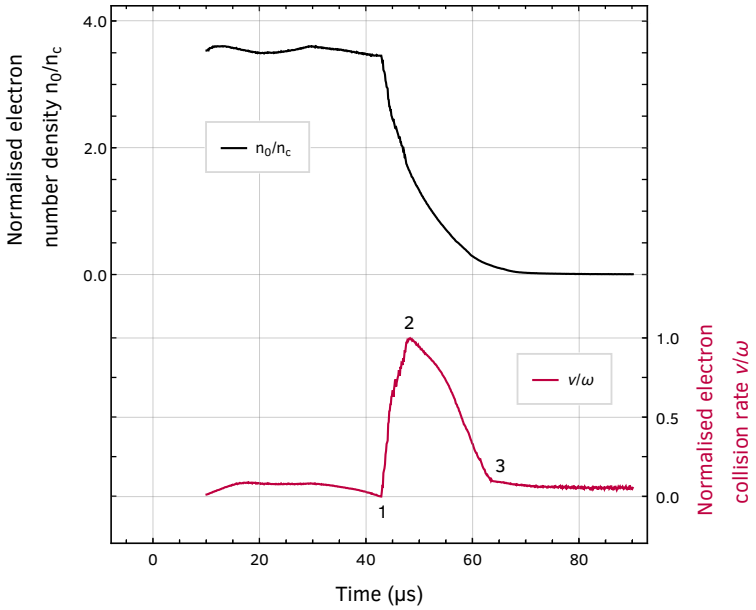

Figure 4.9: High temporal resolution, normalised electron number density and normalised electron collision rate of our transient toroidal helium plasma, as modelled by a uniform torus. Based on complex transmission measurements and full-wave finite-element calculations of our entire experimental set-up, where our toroidal plasma has been mimicked by a torus, these results have been obtained from figure 4.8 by regarding the finite-element calculations as a map for the complex transmission measurements of the toroidal plasma. For our experiment utilising 57 GHz microwave radiation we have $\omega = 3.58\ 10^{11}\ s^{-1}$ and $n_c = 4.03\ 10^{19}\ m^{-3}$.

known values for atmospheric pressure laboratory plasmas.[37]

[37] Kabouzi et al. 2002; F. F. Chen 1974; Richardson 2019.

In the presented evolution of the plasma parameters, discontinuities in the first derivative are clearly visible. These discontinuities are a direct consequence of our choice of splitting the evolution of our toroidal plasma into two parts, and assuming a uniform torus of fixed size for each part. Evidently this is a very course approximation, as the size, and even more importantly, the spatial distribution of the emission from the toroidal plasma, has been seen to evolve considerably. This is supported by the observation that the size of the torus used to mimic our toroidal plasma in the finite-element calculations can have a significant effect on the obtained plasma parameters. Specifically, attributing vastly different plasma parameters $(n_0/n_c,\ \nu/\omega)$ to differently sized tori can result in an almost identical complex transmission coefficient, as can be seen explicitly in figure 4.8 where the calculations for $n_0/n_c = 3.6$ and $\nu/\omega = 0.6$ intersect.

In order to better understand the cause of the discontinuities visible in the electron collision rate presented in figure 4.9, we will briefly discuss these discontinuities in what follows.

(1) This discontinuity arises as a result of the extreme sensitivity of the finite-element calculations on the size of the torus used to model our toroidal plasma. This sensitivity has already been mentioned in the preceding paragraph. In figure 4.8 this discontinuity corresponds precisely to the moment (red label 1) when the measured transmission coefficient leaves the domain in the complex plain spanned by the finite-element calculations for constant electron density (purple, green and blue dotted lines).

(2) When the measured transmission coefficient crosses the finite-element calculations for a constant normalised electron collision rate of 1.0 (blue dot-dashed line and red label 2 in figure 4.8), a discontinuity arises because, before this crossing, the electron collision rate increases after leaving the first discontinuity, and after this crossing, it decreases again, as the measured transmission coefficient continues to move through the domain spanned by the finite-element calculations for a constant electron collision rate (coloured dot-dashed lines). Note that to create a continuous map a linear interpolation has been used.

(3) This discontinuity arises because the measured transmission coefficient enters a region in the complex plane that is not bounded by a series of finite-element calculations, which renders the interpolation unreliable. This could be improved by performing additional finite-element calculations for lower values of the electron collision rate.

In conclusion of this section, we will assess the electron collision

rate presented in figure 4.9. We already noted that in the first half of the evolution of the toroidal plasma, the electron number density is well above cut-off. During this time, microwave radiation cannot significantly penetrate the toroidal plasma, and the resulting electron collision rate should therefore be interpreted with caution.

In the second half of the evolution, the electron collision rate decreases monotonically to a limit value. Because plasma emission is still observed during this time, it is not unreasonable to assume that the electrons still have an elevated temperature while cooling down. But, at the same time, the electron collision rate is seen to decrease a factor of ten. For weakly ionised plasmas the electron collision rate is given by[38]

[38] Richardson 2019, p. 38.

$$\nu = n_n \sigma \sqrt{\frac{kT_e}{m_e}}$$

where n_n is the neutral density, σ is the scattering cross section, k is the Boltzmann constant, T_e is the electron temperature, and m_e is the electron mass. Therefore, we ought to conclude that the electron temperature should have been at least 30.000 K, assuming that the neutral density has already been restored. The latter is a reasonable assumption if we consider the density measurements presented in section 2.5. However, such an electron temperature is unreasonable at this time in the afterglow.[39]

[39] Nedanovska et al. 2015.

If we reconsider the foregoing and bring to mind the optical images of the toroidal plasma presented in section 2.5, we may reasonably conclude that, because the toroidal plasma does not resemble a torus in this part of its evolution, the finite-element calculations cannot be considered representative during this time. As has been mentioned before in this section, considerable improvements can be expected when a tomographically reconstructed, poloidal radiant intensity profile, based on optical recordings, is used as a measure for the dimensions and the electron number density of the toroidal plasma.

4.4 *Conclusion*

In this chapter we have presented the electron number density and the electron collision rate for the entire evolution of a transient toroidal helium plasma. These plasmas have been generated by a single laser-induced breakdown plasma, in quiescent atmospheric pressure helium gas at room temperature, using a laser pulse energy of 250 mJ.

By combining interferometric measurements using 57 GHz microwave radiation with detailed full-wave finite-element calculations of our

interferometric set-up, we were able to obtain the plasma parameters with high temporal resolution.

In the second half of the evolution, where the toroidal plasma can be regarded as an afterglow, the electron number density and the electron collision rate are of the order of 10^{19} m^{-3} respectively 10^{10} s^{-1}, which conforms to known values for atmospheric pressure laboratory plasmas.

We discussed in detail the microwave interferometric set-up used to measure the complex transmission coefficient, and presented a method whereby the finite-element calculations can be used as a map between the measured transmission coefficient and the sought after plasma parameters. With this approach we overcame the biggest challenges in studying transient toroidal helium plasmas, namely their limited lifetime and their limited size.

Because the finite-element calculations already are computationally intensive, we have limited the calculation of the complex transmission coefficient to uniform tori of two sizes that are representative for the evolution of our toroidal plasma. For each of these different sized tori, full-wave finite-element calculations have been performed for a range of values for the complex permittivity.

In the presented evolution of the plasma parameters, discontinuities in the first derivative are clearly visible. These discontinuities are a direct consequence of our choice of splitting the evolution of our toroidal plasma into two parts, and assuming a uniform torus of fixed size for each part. Evidently this is a very course approximation, as the size and the spatial distribution of the emission from the toroidal plasma have been seen to evolve considerably.

We briefly discussed an improvement of this method by which a tomographically reconstructed, poloidal radiant intensity profile, based on optical recordings, can be used as a measure for the dimensions and the electron number density of the toroidal plasma, to better model the toroidal plasma in the finite-element calculations.

Finally, we note that the size of the torus used to mimic our toroidal plasma in the finite-element calculations can have a significant effect on the obtained plasma parameters. Specifically, attributing vastly different plasma parameters to differently sized tori can result in an almost identical complex transmission coefficient. This obviously complicates the method whereby the finite-element calculations are used as a map between the measured transmission coefficient and the sought after plasma parameters. This suggest that considerable improvements can be expected when utilising the aforementioned tomographically reconstructed, poloidal radiant intensity profile.